

# Numerical Heat Transfer, Part A: Applications

## An International Journal of Computation and Methodology

ISSN: 1040-7782 (Print) 1521-0634 (Online) Journal homepage: <http://www.tandfonline.com/loi/unht20>

## Thermal damage during ablation of biological tissues

Bruna R. Loiola, Helcio R. B. Orlande & George S. Dulikravich

To cite this article: Bruna R. Loiola, Helcio R. B. Orlande & George S. Dulikravich (2018) Thermal damage during ablation of biological tissues, Numerical Heat Transfer, Part A: Applications, 73:10, 685-701, DOI: [10.1080/10407782.2018.1464794](https://doi.org/10.1080/10407782.2018.1464794)

To link to this article: <https://doi.org/10.1080/10407782.2018.1464794>



Published online: 04 Jun 2018.



Submit your article to this journal [↗](#)



Article views: 4






View related articles [↗](#)



View Crossmark data [↗](#)



# Thermal damage during ablation of biological tissues

Bruna R. Loiola<sup>a</sup> , Helcio R. B. Orlando<sup>a</sup>  and George S. Dulikravich<sup>b</sup> 

<sup>a</sup>Department of Mechanical Engineering, COPPE, Federal University of Rio de Janeiro (UFRJ), Rio de Janeiro, Brazil; <sup>b</sup>Department of Mechanical and Materials Engineering, MAIDROC Laboratory, Florida International University, Miami, FL, USA

## ABSTRACT

This study presents the numerical solution of a bioheat transfer problem related to the ablation of biological tissues continuously heated by a laser. Different mechanisms of thermal decomposition, such as coagulation, vaporization, and removal of the necrotic tissues, were taken into account in the analysis. The finite volume method was used to obtain the numerical solution of the temperature field, while the volume of fluid method was used to track the ablation interface. Results obtained for cases of practical interest provide a good indication of the area affected by the thermal treatment and are in good agreement with experimental data available in the literature.

## ARTICLE HISTORY



Received 26 December 2017  
Accepted 10 April 2018

## Introduction

Thermal ablation in clinical applications consists of removal or destruction of specific tissue by heat [1–4]. Different heat sources can be used to increase the temperature of biological tissues during thermal ablation, such as radio frequency, ultrasound, microwaves, and lasers at various wavelengths [4–6]. Lasers are normally selected for superficial thermal ablation, because of their compatibility with magnetic resonance devices used for the measurement of the tissue temperature [7]. A rather common disease that affects 80% of men above the age of 75 is benign prostatic hyperplasia [7]. In order to treat this growth of the prostate, a focused laser can be used to destroy the abnormal tissue [7]. In case of cardiac arrhythmias, this kind of procedure can be performed with heating imposed by electromagnetic waves in the radio frequency range, to destroy heart tissues that cause irregular heartbeats [8]. For tumors in the prostate, liver, breast, and pancreas, focused ultrasound is also a common heat source for ablation treatment [9].

Although the classical Pennes model [10] has been used in many bioheat transfer studies, other phenomena, besides metabolism and blood perfusion, need to be accounted for in case of thermal ablation of tissues. These phenomena include water vaporization, blood coagulation, and tissue necrosis. Abraham and Sparrow [11] proposed a bioheat transfer model with the energy equation written in the enthalpy form, which can be used for the different phases that a tissue undergoes during thermal ablation. Also, the perfusion term was considered in reference [11] as function of the tissue thermal damage, based on the works of Henriques and Moritz [12–15].

The thermal damage of tissues is not only a function of the temperatures reached during the treatment, but also of the time that the tissues are exposed to such high temperatures [13]. Therefore, as another kind of medical treatment that aims at the destruction of abnormal cells, such as radiotherapy, a thermal dose needs to be defined to model the damage imposed by heat

**CONTACT** Helcio R. B. Orlando  [helcio@mecanica.coppe.ufrj.br](mailto:helcio@mecanica.coppe.ufrj.br)  Department of Mechanical Engineering, Polit cnica/COPPE, Federal University of Rio de Janeiro (UFRJ), Cid. Universitaria, Cx. Postal: 68503 Rio de Janeiro, RJ, 21941-972, Brazil. Color versions of one or more of the figures in the article can be found online at [www.tandfonline.com/unht](http://www.tandfonline.com/unht).

## Nomenclature

$A$	scale factor, $s^{-1}$	$T_{pre}$	pre-ablation temperature, $^{\circ}C$
$c_p$	specific heat at constant pressure, $J/kg/K$	$T_{sat}$	saturation temperature, $^{\circ}C$
$C_{liq}$	water fraction in the tissue	$T_w$	wall temperature, $^{\circ}C$
$d$	diameter, m	$\mathbf{V}$	moving boundary velocity vector
$E_a$	energy of activation, $J/mole$	$V_r$	radial velocity, m/s
$f$	volume fraction	$V_z$	longitudinal velocity, m/s
$g$	anisotropy coefficient	<b>Greek symbols</b>	
$h$	enthalpy per unit mass, $J/kg$	$\alpha_v$	thermal diffusivity, $m^2/s$
$h_{\infty}$	heat transfer coefficient, $W/m^2/K$	$\delta$	interface position, m
$h_{fg}$	latent heat, $J/kg$	$\lambda$	wavelength, m
$H$	height of the geometry, m	$\mu_a$	radiation absorption coefficient, $m^{-1}$
$H_{ab}$	heat of ablation, $J/kg$	$\mu_{eff}$	radiation attenuation coefficient, $m^{-1}$
$k$	thermal conductivity, $W/m/K$	$\mu_s$	radiation scattering coefficient, $m^{-1}$
$m_f$	mass fraction of fat	$\xi$	collagen shrinkage
$m_p$	mass fraction of protein	$\rho$	density, $kg/m^3$
$m_w$	mass fraction of water	$\rho_l$	liquid density, $kg/m^3$
$n$	slope of the line	$\omega$	perfusion coefficient, $s^{-1}$
$P$	power, W	$\Omega$	injury integral
$q_{ab}$	heat flux absorbed by the ablating surface, $W/m^2$	<b>Subscripts</b>	
$Q$	heat source per unit volume, $W/m^3$	0	initial time
$r, z$	spatial coordinates	$ab$	ablation
$r^*, z^*$	position of the moving boundary surface	$b$	blood
$R$	radius of the geometry, m	$l$	laser
$R_0$	internal radius of the geometry, m	$m$	metabolism
$R_u$	universal gas constant, $J/mole/K$	<b>Subscripts</b>	
$S$	fraction of surviving cells	—	refers to tissue properties before phase change
$t$	time	+	refers to tissue properties after phase change
$T$	temperature, $^{\circ}C$		
$T_{\infty}$	external bulk temperature, $^{\circ}C$		

to the biological tissues [16]. The thermal damage may be analyzed by means of protein denaturation, cell death, coagulation, and necrosis of the tissues [17].

Proteins can be found in the body in globular, fibrosis, or membrane forms [17]. The main protein in the composition of different organs is collagen. Therefore, one way to study the protein denaturation is to analyze modifications in collagen, such as shrinkage or loss of birefringence [18,19]. Weir [20] analyzed the protein denaturation of collagen in tendons of kangaroos, where an Arrhenius-type expression was used to model the collagen shrinkage. On the other hand, Chen et al. [21] have proposed a model for the collagen shrinkage as a combination of three linear correlations between shrinkage and time when analyzing their experimental data. Their model provided good correlation of the data of Chen et al. [22] for bovine tendons. Similarly, Wall et al. [23] analyzed the bovine tendon collagen shrinkage percentage as a function of temperature changes in a surrounding saline bath and also of the time required by the tissue to reach the bath temperature. Pearce et al. [24] analyzed the protein denaturation by loss of birefringence in rat bowel due to laser heating, by considering an Arrhenius model.

For modeling thermal damage in terms of cell death, several authors [19,25–28] have resorted to a first-order kinetics reaction model for the fraction of surviving cells. Feng et al. [29] developed a two-state model (viable and damage cells) for the *in-vitro* PC3 (human prostate cancer) and RWPE (normal) cell surviving curves during hyperthermia imposed by a constant temperature water bath. O'Neill et al. [30] have proposed a three-state model, represented in terms of state variables given by the numbers of surviving cells, vulnerable cells, and dead cells. In this model, the damage to the cells was analyzed during the treatment (fast cell death) and post-treatment incubation (slow cell death).

The damage to the tissue involves several complex processes. The primary effects that can be observed in *ex-vivo* and *in-vivo* tissues are as follows: water vaporization, caramelization, carbonization, and ablation (crater formation) [14]. Other effects can be observed only during *in-vivo* experiments, such as coagulation and necrosis due to the blood flow blockage [14]. Thermal damage to tissues heated by point heat sources can be observed through thermal markers due to pathological modifications [31,32]. From the heat source center to the periphery, one can find the lesion crater, a carbonization/caramelization layer, a water-depleted region, and a white coagulation zone (due to birefringence loss and collagen hyalinization) [31,32]. Besides that, for *in-vivo* experiments, it is also possible to observe a red band associated with the blood coagulation, as well as a necrosis zone [31,32]. In order to describe these effects, models of thermal damage at the tissue level usually involve an Arrhenius-type formulation [12–18].

The purpose of this study is to present the numerical solution of a two-dimensional, axisymmetric bioheat transfer problem in a biological tissue continuously heated by a laser. The tissue temperature can be raised to values that result in tissue removal by ablation [33]. Before the tissue is removed, it is thermally decomposed and water is vaporized. All these phenomena are appropriately accounted for in the mathematical model used in this work. The formulation for the problem is based on Pennes model written in the enthalpy form [11], which is solved by the finite volume method [34,35]. A moving boundary problem is established when the tissue surface reaches a specified ablation temperature [33] and the volume of fluid (VOF) method is then used to track the ablation front [36]. The numerical code developed in this work was verified against other solutions available in the literature for moving boundary problems [37,38]. The numerical solution obtained for a case of practical interest was verified by following the ASME Verification and Validation standard [35,39,40]. Moreover, experimental results available in the literature [16,32] were used for the code validation.

## Physical problem and mathematical formulation

In order to analyze the thermal ablation and the resulting thermal damage of biological tissues, a two-dimensional problem with axial symmetry is considered here in cylindrical coordinates ( $r, z$ ), as shown in Figure 1. The top surface of the tissue at  $z = H$  is heated by a vertical laser beam having a Gaussian intensity distribution. The top surface also loses heat by convection and linearized radiation to the surrounding environment. First kind boundary conditions are assumed at  $z = 0$  and at  $r = R$ , which are considered at the arterial blood temperature,  $T_b$ . The initial temperature

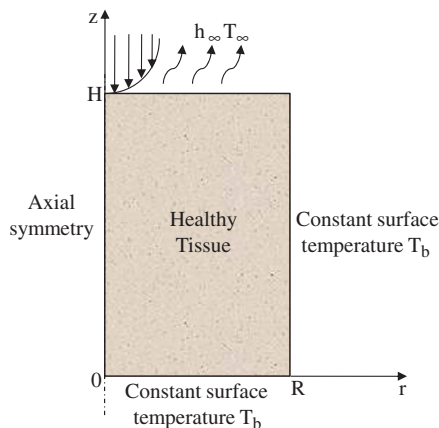


Figure 1. Physical problem.

in the medium is also assumed as  $T_b$ . The tissue is assumed as an isotropic medium, where the physical properties may vary locally as a result of the vaporization of the water inside the tissue.

The physical problem of bioheat transfer was modeled here with an enthalpy form of Pennes model, given by:

$$\rho(r, z) \frac{\partial h(r, z, T)}{\partial t} = \nabla \cdot [k(r, z) \nabla T(r, z, t)] + Q(r, z, T) \quad \text{in } 0 < r < R, \quad 0 < z < H, \quad t > 0 \quad (1.a)$$

$$T(r, z, t) = T_b \quad 0 < r < R \quad 0 < z < H \quad t = 0 \quad (1.b)$$

$$\frac{\partial T(r, z, t)}{\partial r} = 0 \quad r = 0 \quad 0 < z < H \quad t > 0 \quad (1.c)$$

$$T(r, z, t) = T_b \quad r = R \quad 0 < z < H \quad t > 0 \quad (1.d)$$

$$T(r, z, t) = T_b \quad 0 < r < R \quad z = 0 \quad t > 0 \quad (1.e)$$

$$-k(r, z) \frac{\partial T(r, z, t)}{\partial z} = h_\infty (T - T_\infty) \quad 0 < r < R \quad z = H \quad t > 0 \quad (1.f)$$

The enthalpy is related to the temperature as follows [11]:

$$h = \begin{cases} c_p^-(r, z) [T(r, z, t) - T_b] & 37^\circ\text{C} \leq T \leq 99^\circ\text{C} \\ h(99) + h_{fg} C_{liq} \frac{T(r, z, t) - 99}{(100 - 99)} & 99^\circ\text{C} < T \leq 100^\circ\text{C} \\ h(100) + c_p^+(r, z) [T(r, z, t) - 100] & T > 100^\circ\text{C} \end{cases} \quad (2)$$

where the evaporation of the water in the tissue is assumed to occur between  $99^\circ\text{C}$  and  $100^\circ\text{C}$ . In Eq. (2),  $C_{liq}$  is the fraction of water in the tissue.

The heat source is given by the perfusion term,  $Q_b(r, z, T)$ , the metabolic term,  $Q_m(r, z)$ , and the laser heat source,  $Q_l(r, z)$ , that is,

$$Q(r, z, T) = Q_b(r, z, T) + Q_m(r, z) + Q_l(r, z) \quad (3)$$

The perfusion term is given by [10,11]:

$$Q_b(r, z, T) = \rho_b c_b \omega_b(\Omega) [T_b - T(r, z, t)] \quad (4)$$

where the blood perfusion coefficient is considered dependent of the tissue thermal damage,  $\Omega$  [11]. The metabolic heat source  $Q_m(r, z)$  may vary spatially, depending on the tissue. The heating of the tissue by the laser is considered as a volumetric phenomenon, in which the light propagation in the medium is computed with Beer–Lambert's formulation [41]. Thus, the energy absorbed by the tissue is accounted for by considering the laser with a Gaussian beam (spot radius equal to  $2\sigma$ ), irradiance ( $\Phi_0$ ), and the effective attenuation coefficient ( $\mu_{eff}$ ) as:

$$Q_l = \mu_{eff} \Phi_0 \exp[-\mu_{eff}(H - z)] \exp\left(-\frac{r^2}{2\sigma^2}\right) \quad (5)$$

The effective attenuation coefficient  $\mu_{eff}$  is given as a function of the absorption coefficient ( $\mu_a$ ), the scattering coefficient ( $\mu_s$ ), and anisotropy coefficient ( $g$ ) [42], that is,

$$\mu_{eff} = \{3\mu_a[\mu_a + \mu_s(1 - g)]\}^{0.5} \quad (6)$$

The mathematical formulation for the physical problem given by Eqs. (1) to (6) holds for the pre-ablation period, while the temperatures in the domain are smaller than the ablation

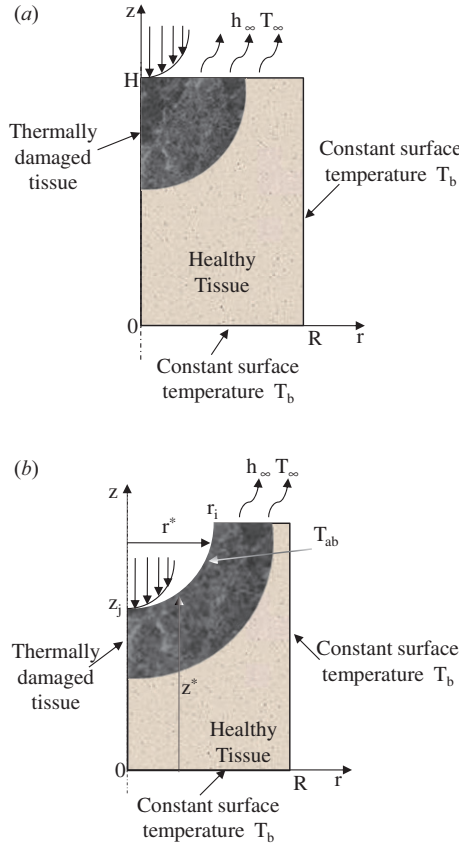


**Figure 2.** (a) Pre-ablation period and (b) moving boundary problem after ablation begins.

temperature,  $T_{ab}$  (see [Figures 1](#) and [2a](#)). A moving boundary problem is then established when the top surface temperature reaches the ablation temperature, as shown in [Figure 2b](#).

The initial condition for the ablation process is given by the temperature field at the end of the pre-ablation period. During ablation, the energy balance at the moving boundary is given by:

$$\rho(r^*, z^*) H_{ab} \mathbf{V}(r^*, z^*) = q_{ab} - k(r^*, z^*) \nabla T(r^*, z^*, t) \quad (7)$$

where  $H_{ab}$  is the heat of ablation,  $\mathbf{V}$  is the boundary velocity, and  $q_{ab}$  is the heat flux at the ablating surface. The laser energy is considered to be fully absorbed at the surface after ablation begins. The moving boundary is specified by the position vector  $(r^*, z^*)$  (see [Figure 2b](#)). From [Eq. \(7\)](#), the ablating surface velocity components in the  $r$  and  $z$  directions considering the heat flux in each direction,  $q_r$  and  $q_z$ , can be, respectively, calculated as:

$$V_r = \frac{1}{\rho H_{ab}} \left[ q_r - k(r^*, z^*) \frac{\partial T(r^*, z^*)}{\partial r} \right] \quad (8.a)$$

$$V_z = \frac{1}{\rho H_{ab}} \left[ q_z - k(r^*, z^*) \frac{\partial T(r^*, z^*)}{\partial z} \right] \quad (8.b)$$

## Models for the thermal decomposition of the tissues

The models used in this work to predict the thermal decomposition of the tissues include those that consider protein denaturation by birefringence loss [\[18\]](#) and cell death [\[29\]](#).

**Table 1.** Parameters used for the thermal damage analysis.

Number	Model	Parameters	Reference
1	Arrhenius, Eq. (9)	$A = 1.606 \times 10^{45} \text{ s}^{-1}$ ; $E_a = 3.06 \times 10^5 \text{ J mol}^{-1}$	[18]
2	Arrhenius, Eq. (9)	$A = 1.19 \times 10^{35} \text{ s}^{-1}$ ; $E_a = 2.318 \times 10^5 \text{ J mol}^{-1}$	[29]
3	Two-state, Eq. (11)	$\alpha = 0.00493 \text{ s}^{-1}$ ; $\beta = 215.64$ ; $\gamma = 70,031 \text{ K}$	[29]

The dimensionless damage ( $\Omega$ ) to the tissue is usually predicted by an Arrhenius expression [12–15]:

$$\Omega = \int_0^t A e^{\left(-\frac{E_a}{R_u T}\right)} dt \quad (9)$$

where  $E_a$  is the activation energy,  $A$  is the scale factor ( $A$ ), and  $R_u$  is the universal gas constant.

The dimensionless damage can be correlated to cell death and to the collagen birefringence loss by [16–19]:

$$\Omega = \ln \left\{ \frac{S(0)}{S(t)} \right\} = \ln \left\{ \frac{I_B(0)}{I_B(t)} \right\} \quad (10)$$

where  $S(t)$  represents the fraction of surviving cells and  $I_B(t)$  is the birefringence intensity. The value  $\Omega = 1$  is commonly used to indicate tissue damage that represents a second-degree burn [12–15], that is, 63.2% of dead cells or birefringence loss [18,19]. Thus, the blood perfusion coefficient and the metabolic heat source are considered null after the tissue is thermally damaged ( $\Omega = 1$ ).

The work of Pearce et al. [18] is used here to predict the thermal damage in terms of birefringence loss. Pearce et al. [18] have analyzed the protein denaturation by birefringence loss in rat skin during *in-vitro* experiments, at temperatures between 40 °C and 90 °C in a water bath, for heating periods between 120 s and 6,000 s. They measured the birefringence intensity ( $I_B$ ) with a transmission polarizing microscope and correlated their results by using Eq. (9) with  $A = 1.606 \times 10^{45} \text{ s}^{-1}$  and  $E_a = 3.06 \times 10^5 \text{ J mol}^{-1}$ .

Feng et al. [29] developed a two-state model for the PC3 (human prostate cancer) and RWPE (normal) cell surviving curves, for hyperthermia *in-vitro* experiments in the range of 44 °C to 60 °C and exposure durations of 1–30 min [29]. The cell survival curve fit given by

$$S(t, T) = \frac{1}{1 + e^{-\left[\frac{\gamma}{T} - \beta - \alpha t\right]}} \quad (11)$$

with  $\alpha = 0.00493 \text{ s}^{-1}$ ,  $\beta = 215.64$ , and  $\gamma = 70,031 \text{ K}$  provided good correlation of the experimental data for the PC3 cells. Similarly, the authors correlated their experimental results in terms of the Arrhenius model with the following parameters:  $A = 1.19 \times 10^{35} \text{ s}^{-1}$  and  $E_a = 2.318 \times 10^5 \text{ J mol}^{-1}$ . The models and their associated parameters used in this work are shown in Table 1.

## Numerical method of solution

The temperature field was calculated with the finite volume method [34], in the pre-ablation and ablation periods, by using the enthalpy formulation given by Eqs. (1)–(6). The explicit enthalpy scheme was used for the numerical solution [35].

In order to solve the problem during the ablation period, the position of the moving boundary was tracked with the VOF method originated by Hirt and Nichols [36]. In this method, the moving surface is approximated by a straight line inside each finite volume. A parameter  $f$  is used to indicate the volume fraction occupied by the tissue in each of these control volumes, where  $f = 0$  indicates that the volume is empty, that is, the tissue was fully removed by the ablation process.

A value of  $f=1$  indicates that the volume is completely filled by the tissue, while a value of  $f$  between 0 and 1 indicates that the surface is moving through the volume. To approximate the surface by a straight line inside each finite volume with  $0 < f < 1$ , it is necessary to find its slope and the points where it intercepts the volume boundaries. Youngs approach [43] was applied in this work, where the boundary slope was obtained from the tissue volume fraction normalized gradient direction, calculated as:

$$\mathbf{n} = \frac{\nabla f}{|\nabla f|} \quad (12)$$

The gradient in each direction is obtained with finite difference approximations as follows:

$$\frac{\partial f}{\partial r} = \frac{f_E - f_W}{2\Delta r} \quad (13.a)$$

$$\frac{\partial f}{\partial z} = \frac{f_N - f_S}{2\Delta z} \quad (13.b)$$

where the subscripts follow the classical notation for finite volumes. The fractions  $f_E$ ,  $f_W$ ,  $f_N$ , and  $f_S$  computed over a uniform grid for this problem are given by [44]:

$$f_E = \frac{f_{(i+1,j-1)} + 2f_{(i+1,j)} + f_{(i+1,j+1)}}{4} \quad (14.a)$$

$$f_W = \frac{f_{(i-1,j-1)} + 2f_{(i-1,j)} + f_{(i-1,j+1)}}{4} \quad (14.b)$$

$$f_N = \frac{f_{(i-1,j+1)} + 2f_{(i,j+1)} + f_{(i+1,j+1)}}{4} \quad (14.c)$$

$$f_S = \frac{f_{(i-1,j-1)} + 2f_{(i,j-1)} + f_{(i+1,j-1)}}{4} \quad (14.d)$$

where the subscripts  $i$  and  $j$  indicate the volumes at  $r = i\Delta r$  and  $z = j\Delta z$ .

The points where the surface intercepts the control volume boundaries are found by applying the conservation of mass inside each finite volume that contains the boundary surface. The volume fraction satisfies the following advection equation [36] that is solved with an upwind finite-difference scheme [34,35]:

$$\frac{\partial f}{\partial t} + \frac{V_r}{r} \frac{\partial(rf)}{\partial r} + V_z \frac{\partial f}{\partial z} = 0 \quad (15)$$

## Results and discussions

The finite volume code developed in this work, which makes use of the VOF method for tracking the moving surface after the tissue removal starts, was verified by using solutions available in the literature. After the code verification, the solution verification procedure specified by ASME [40] was applied for test cases involving different laser diameters and laser powers. Finally, the code was validated against experimental results available in the literature for the ablation of rat liver with Nd:YAG laser [16,32]. The numerical codes were implemented in MATLAB<sup>®</sup> and run in a computer having 64 bits, Windows 10, processor Intel<sup>®</sup> Core<sup>™</sup>i7-7500U CPU@2.70Ghz 2.90 GHz and with 16GB of RAM.

### Code verification

Two different test cases were used for the verification of our numerical code by considering one-dimensional moving boundary problems in the radial and in the longitudinal directions.



**Table 2.** Input data for the verification with the work of Welch and Wilson [37].

Input data	Values
$\rho_f$	957.854 kg/m <sup>3</sup>
$P$	0.5956 kg/m <sup>3</sup>
$c_p$	2,017 J/(kg·K)
$K$	0.0248 W/(m·K)
$\alpha_v$	$2.0644 \times 10^{-5}$ m <sup>2</sup> /s
$H_{ab}$	2,257 kJ/kg
$T_{sat}$	373.15 K
$T_w$	398.15 K
$R_0$	100 m
$R-R_0$	0.040 m
$H$	0.040 m

The article of Welch and Wilson [37] was used for the code verification in the radial direction. In this work, liquid water at the saturation temperature ( $T_{sat}$ ) and atmospheric pressure fills a one-dimensional region in Cartesian coordinates. Liquid is then exposed to a constant temperature ( $T_w$ ) higher than the saturation temperature at one of the boundaries, so that vapor is formed and the vapor–liquid interface moves into the liquid region. Welch and Wilson [37] solved this one-dimensional problem with the finite volume method and the VOF method was used to track the vapor–liquid interface. The numerical results were compared to an analytical solution for the problem. For the verification of our code with the results of Welch and Wilson [37], the phase change problem described above was solved in a hollow cylinder, with thermally insulated top and bottom boundaries and with large internal radius ( $R_0$ ) and small thickness, so that the effects of curvature could be neglected. The internal surface at  $r = R_0$  was maintained at a constant temperature larger than the saturation temperature, while the external surface was maintained at the initial saturation temperature. Both phases were considered incompressible and the vapor was considered motionless. The data used in this verification are shown in Table 2. Our numerical solution was computed with a uniform mesh of  $40 \times 40$  finite volumes, a time step of 0.01 s and a final time of 1,600 s. The results obtained with our code are compared to the numerical and analytical results of Welch and Wilson [37] for the vapor–liquid interface position in Figure 3. The maximum relative error between our numerical results and the analytical solution was 0.0014%, demonstrating that the agreement of our results with the analytical solution was better than that of the numerical results of Welch and Wilson [37].

The verification of our code in the longitudinal direction was performed with a one-dimensional problem involving the ablation of Teflon [38]. The lateral surface of the cylindrical region at  $r = R$  and the bottom boundary at  $z = 0$  were thermally insulated, while the top boundary at  $z = H$  was subjected to a constant and uniform heat flux,  $q_{ab}$ . The initial temperature ( $T_0$ ) in the region was uniform. Ablation was supposed to start when the top boundary reached the ablation temperature ( $T_{ab}$ ) and then a moving boundary problem was established. Ruperti and Cotta [38] solved this problem by using the generalized integral transform technique. The input data used for this verification are shown in Table 3 [38]. The numerical solution was obtained with a uniform mesh of  $40 \times 40$  finite volumes, a time step of 0.01 s, and a final time of 1,064 s. Figure 4 presents our numerical solution and the results obtained by Ruperti and Cotta [38]. The maximum relative error between our numerical results and the solution of Ruperti and Cotta [38] was 2.6%.

### Solution verification

After the verification of our code in the longitudinal and radial directions, we proceeded with the solution verification, based on the procedure established by ASME [39,40], in a case of practical interest for which reference solutions are not available. Our numerical solution was computed

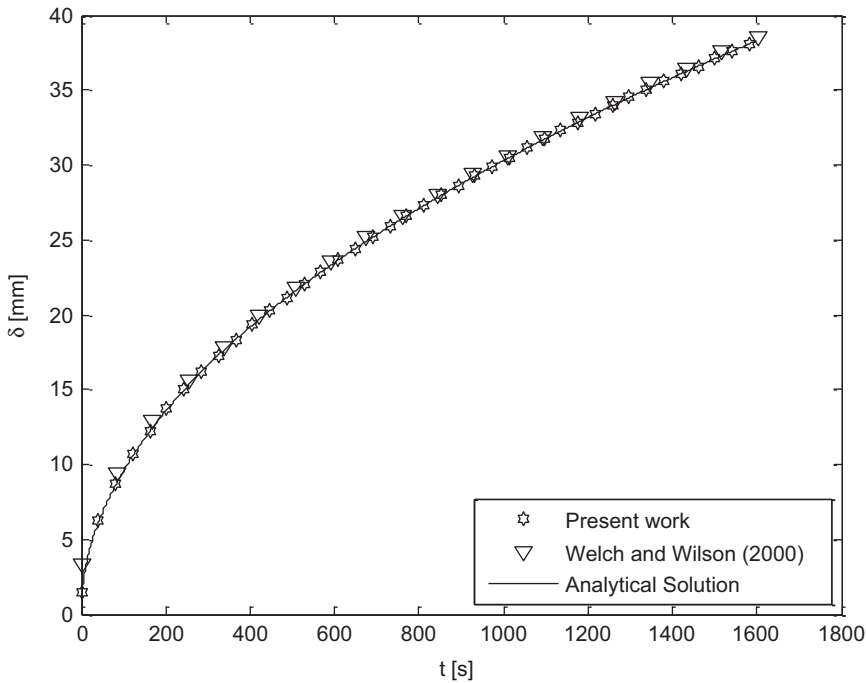


**Figure 3.** Interface position – verification with the work of Welch and Wilson [37].

**Table 3.** Input data for the verification with the work of Ruperti and Cotta [38].

Input data	Values
$\rho$	1,922 kg/m <sup>3</sup>
$c_p$	1,256 J/(kg-K)
$k$	0.22 W/(m-K)
$T_0$	25 °C
$T_{ab}$	560 °C
$q''_{ab}$	23,540 W/m <sup>2</sup>
$H_{ab}$	671,960 J/kg
$R$	0.040 m
$H$	0.040 m

with different meshes for the input data shown in Table 4. For the results presented below for the moving boundary problem resulting from the ablation of biological tissues, the values of thermal properties similar to those of human skin were used, with a composition of 65% of water ( $m_w = 0.65$ ) and 35% of protein ( $m_p = 0.35$ ) [45]. The properties of the biological tissue were calculated with the following expressions [19,46]:

$$\rho = \frac{1}{m_w + 0.649m_p + 1.227m_f} \quad (16.a)$$

$$c_p = 4.2m_w + 1.09m_p + 2.3m_f \quad (16.b)$$

$$k = \rho(6.28m_w + 1.17m_p + 2.31m_f) \quad (16.c)$$

The optical properties were obtained from Pearce [19,47], while the blood properties were obtained from Abraham and Sparrow [11]. Water and air properties were obtained from [50,51] (see Table 4). Two different laser powers were considered for the results presented below,  $P = 1$

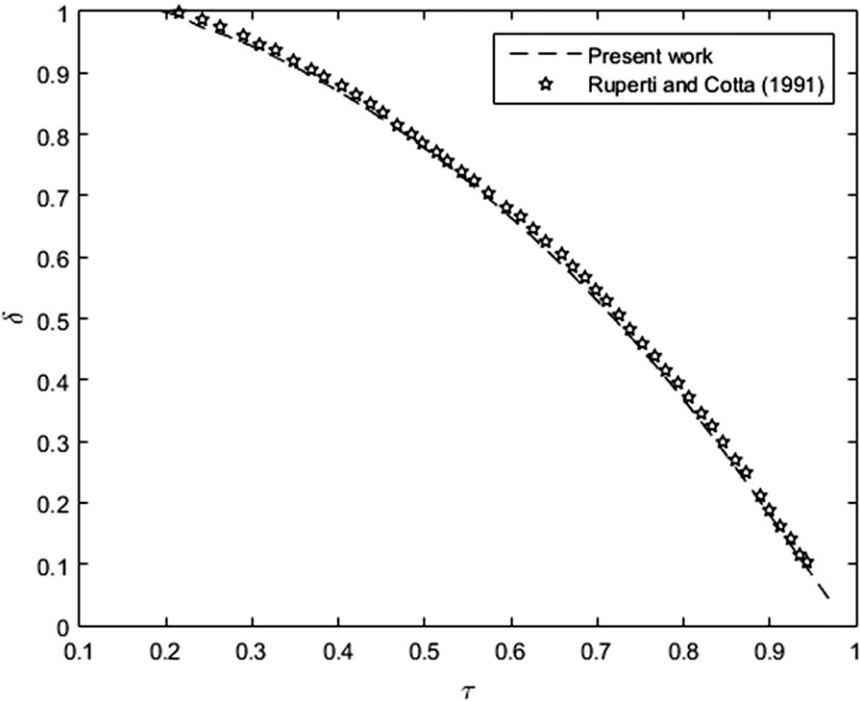


Figure 4. Interface position – verification with the work of Ruperti and Cotta [38].

Table 4. Input data used for the solution verification.

Properties	Values	Reference
$\rho^-$	1,140 kg/m <sup>3</sup>	[46]
$\rho^+$	4,400 kg/m <sup>3</sup>	[46]
$c_p^-$	3,110 J/(kg-K)	[46]
$c_p^+$	382 J/(kg-K)	[46]
$k^-$	0.512 W/(m-K)	[46]
$k^+$	0.180 W/(m-K)	[46]
$\rho_b$	1,000 kg/m <sup>3</sup>	[11]
$c_b$	4,100 J/(kg-K)	[11]
$\omega_0$	0.0028 s <sup>-1</sup>	[11]
$T_b$	37 °C	[11]
$T_{ab}$	180 °C	[33]
$H_{ab}$	2,015 kJ/kg	[50]
$h_{fg}$	2,257 kJ/kg	[50]
$C_{liq}$	0.65	[45]
$Q_m$	170 W/m <sup>3</sup>	[11]
$\mu_{eff}$	4,060 m <sup>-1</sup>	[19]
$h_\infty$	10 W/(m <sup>2</sup> -K)	[51]
$T_\infty$	25 °C	[51]
$R$	0.007 m	–
$H$	0.007 m	–

W and  $P=10$  W. The effects of the laser beam radius were analyzed, by considering  $\sigma=0.3$  mm and  $\sigma=0.5$  mm, where the maximum flux at the center of the beam is given by:

$$\Phi_0 = \frac{P}{2\pi\sigma^2} \tag{17}$$

The discrepancies between numerical results obtained with different meshes were calculated in order to identify an asymptotic behavior of the discretization error for the four cases involving

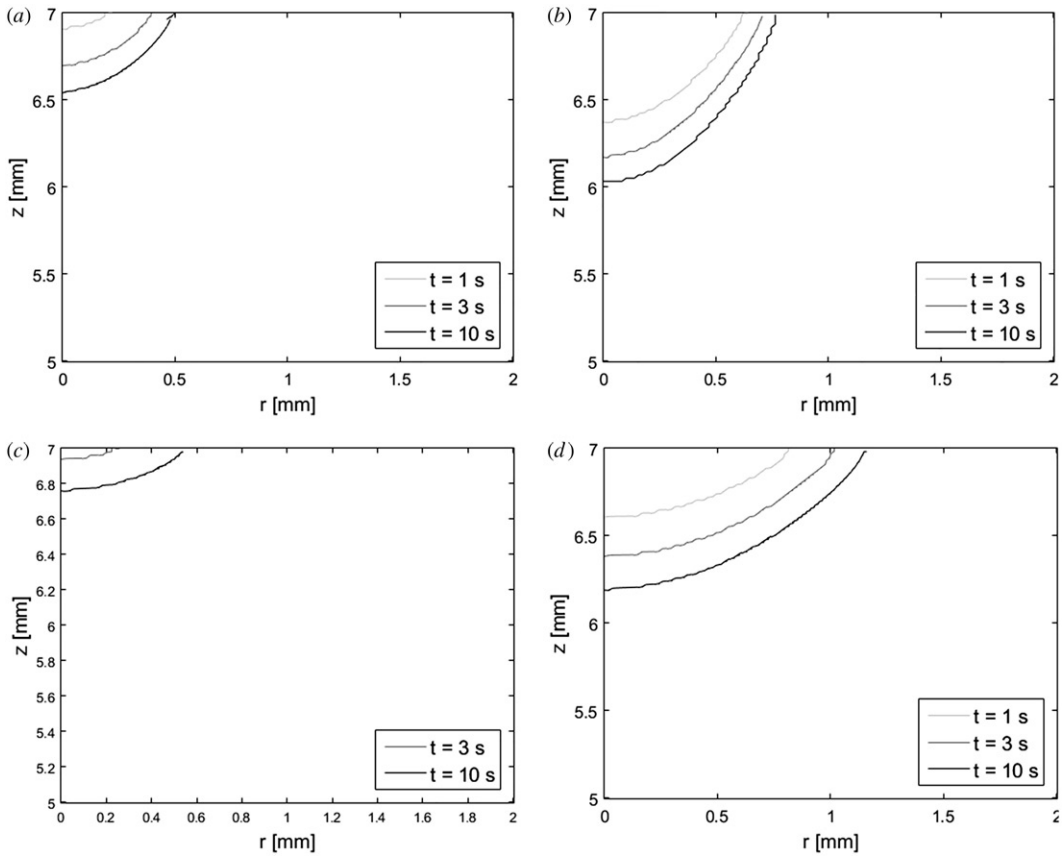


**Figure 5.** Shape of the crater lesion for different times (1 s, 3 s, and 10 s) using a laser of (a) 1 W and  $d = 1.2$  mm ( $\sigma = 0.3$  mm), (b) 10 W and  $d = 1.2$  mm ( $\sigma = 0.3$  mm), (c) 1 W and  $d = 2$  mm ( $\sigma = 0.5$  mm), and (d) 10 W and  $d = 2$  mm ( $\sigma = 0.5$  mm).

different laser powers and laser beams mentioned above. With the mesh refinement, it was possible to calculate the discretization error order ( $p$ ), as well as an extrapolated solution and its associated grid convergence index (GCI), with the three most refined meshes. The mesh size used for the refinement analysis was  $\sqrt{\Delta r \Delta z}$ , which was successively reduced by a factor of 1.5 [40]. The time steps for each mesh were chosen based on stability requirements. The meshes with 380, 570, and 855 control volumes in each direction were considered to behave asymptotically during the pre-ablation period, with time steps of  $2 \times 10^{-4}$  s for the two least refined meshes and  $5 \times 10^{-5}$  s for the most refined mesh. The discrepancies between meshes with successive degrees of refinement were computed for the temperatures at  $r = 0$  and at  $z = H$ , because these regions involved large temperature gradients. Based on such quantities, the average convergence order was  $p = 3.55$ , the maximum GCI was  $0.05^\circ\text{C}$ , while the maximum discrepancy between the meshes with 380 and 570 control volumes in each direction was  $0.06^\circ\text{C}$ . Since the maximum GCI was practically the same as the maximum discrepancy between the two least refined meshes, the mesh with 380 control volumes in each direction was used for the results presented below. Moreover, this mesh involved the shortest computing times, which were of 8.5 minutes, 16.7 minutes, and 3.6 hours for the meshes with 380, 570, and 855 control volumes in each direction, respectively, during the pre-ablation period, with  $P = 1$  W and  $\sigma = 0.3$  mm.

The ablation lesions were analyzed for two different laser powers (1 W and 10 W) and two different laser beam diameters (1.2 mm and 2.0 mm). Figure 5 presents the positions of the ablation

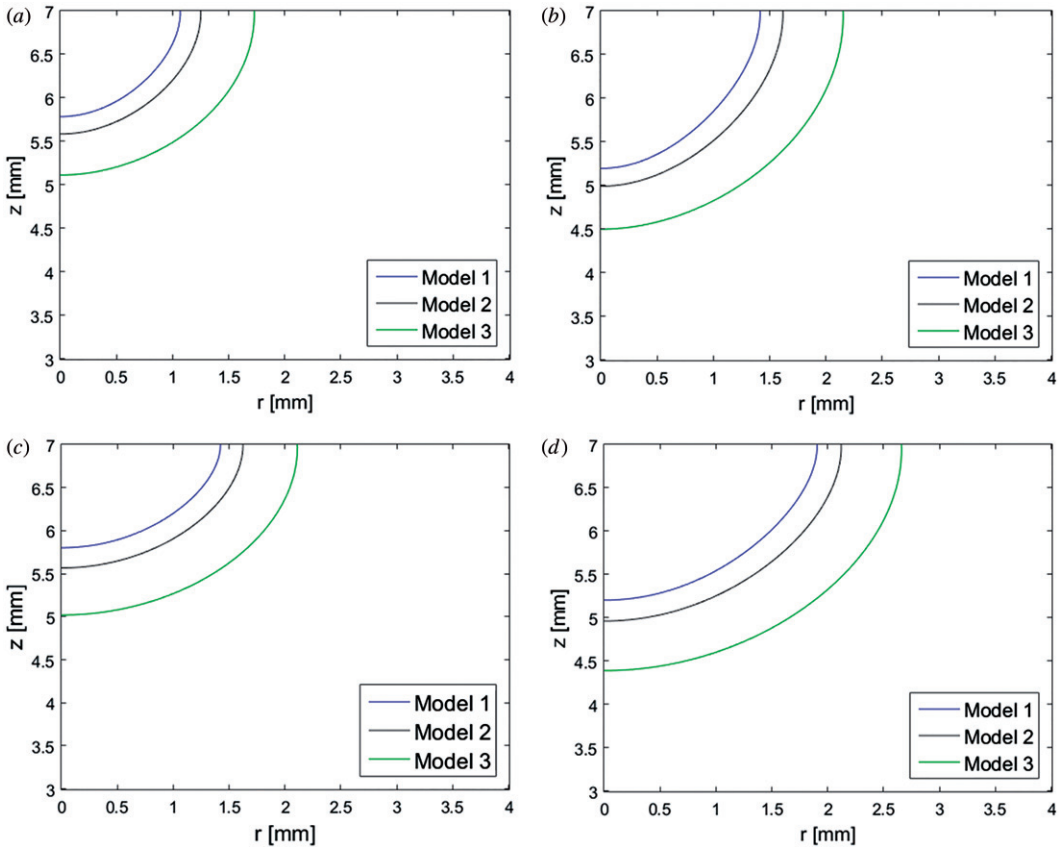


**Figure 6.** Thermal damage contours ( $\Omega=1$ ) after heating the biological tissue for 10 s using different laser powers and beam spot diameters: (a) 1 W and  $d=1.2$  mm ( $\sigma=0.3$  mm), (b) 10 W and  $d=1.2$  mm ( $\sigma=0.3$  mm), (c) 1 W and  $d=2$  mm ( $\sigma=0.5$  mm), and (d) 10 W and  $d=2$  mm ( $\sigma=0.5$  mm).

front at times 1 s, 3 s, and 10 s, for different combinations of laser powers and diameters. For the same power, the penetration depth increased by reducing the beam spot diameter, as shown in Figure 5a,c for the power of 1 W, and also in Figure 5b,d for the power of 10 W. Such is the case because the imposed heat flux increased by reducing the beam spot diameter. Figure 5a–5d also shows that the size of the lesion increased with the laser power. An analysis of the thermal damage was also performed for this case, by using the models summarized in Table 1. The classical value of the damage integral  $\Omega=1$  was used to determine the thermal damage to the tissue [12–15]. The contours for  $\Omega=1$ , which separate the thermally damaged and undamaged regions, are shown in Figure 6, at time  $t=10$  s. This figure shows that the depth of the thermally damaged region at  $z=0$  was not significantly affected by the laser power. However, the width of the necrotic region increased with the laser beam diameter and also with the laser power. The results presented in Figure 6 revealed that the thermally damaged region predicted with model 3 was the largest, followed by those predicted with the Arrhenius models 2 and 1 (see Table 1).

### Validation

In order to perform the validation of our numerical code, the numerical results obtained here were compared with the experimental results available in the literature by Thomsen and Pearce [16,32]. In these works, *in-vivo* rat liver was heated by a Nd:YAG laser with wavelength of 1,064 nm. The results used in the validation were obtained with a laser diameter of 2 mm, power

**Table 5.** Input data used for the validation.

Input data	Values	Reference
$\rho^-$	1,076 kg/m <sup>3</sup>	[46]
$\rho^+$	1,541 kg/m <sup>3</sup>	[46]
$c_p^-$	3,578 J/(kg-K)	[46]
$c_p^+$	1,090 J/(kg-K)	[46]
$k^-$	0.565 W/(m-K)	[46]
$k^+$	0.180 W/(m-K)	[46]
$\rho_b$	1,000 kg/m <sup>3</sup>	[11]
$c_b$	4,100 J/(kg-K)	[11]
$\omega_0$	0.0028 s <sup>-1</sup>	[11]
$T_b$	37 °C	[11]
$T_{ab}$	180 °C	[33]
$H_{ab}$	2,015 kJ/kg	[50]
$h_{fg}$	2,257 kJ/kg	[50]
$C_{liq}$	0.80	[31]
$Q_m$	170 W/m <sup>3</sup>	[11]
$\mu_{eff}$	1,380 m <sup>-1</sup>	[48]
$h_\infty$	10 W/(m <sup>2</sup> -K)	[51]
$T_\infty$	25 °C	[51]
$P$	9 W	[32]
$\sigma$	0.5 mm	[32]
$\varphi_0$	573 W/cm <sup>2</sup>	[24]
$R$	0.010 m	–
$H$	0.010 m	–

of 9 W, and an exposure time of 10 s. The optical properties of rat liver at 1,064 nm used in this work were obtained from Parsa et al. [48]. The rat liver tissue was considered with water fraction of 80% and protein fraction of 20% [31]. The thermal properties took into account the vaporization of water in the tissues, as proposed by Cooper and Trezek [46] (see Eqs. 16a–16c). The blood properties were considered as the same used by Abraham and Sparrow [11]. The input values used in the numerical simulation are shown in Table 5. The geometry was considered as a cylinder of 10 mm in height and 10 mm in radius, which was discretized with 543 uniform control volumes in each direction. The numerical solution was obtained with a time step of 0.0002 s.

The numerical solution obtained in this work for the ablation front was superimposed over the experimental result presented by Thomsen and Pearce [16] in Figure 7a. Despite the fact that the original geometry of the rat liver is not a homogeneous cylinder, as considered for the numerical solution, the ablation front computed with our numerical code shows an excellent agreement with the experimental lesion [16]. This figure shows that not only the actual front location, but also its shape, were very accurately predicated with our numerical code. The tissue thermal damage contours, obtained with  $\Omega = 1$  and with the three models used in this work (see Table 1), were superimposed with the experimental result presented by Thomsen and Pearce [16] in Figure 7b. However, in this case, model 2 was set with the values  $A = 2.09 \times 10^{45} \text{ s}^{-1}$  and  $E_a = 2.219 \times 10^5 \text{ J/mol}$  for rat liver [49]. It was expected that models 1 and 2 would more appropriately represent the white coagulation zone, while model 3 would more appropriately represent the necrotic zone (dark region) [31], due to the temperatures associated with the contours  $\Omega = 1$  for each model. These temperatures were 78 °C, 70 °C, and 52.5 °C, for models 1, 2, and 3, respectively. Although models 1 and 2 predicted the white coagulation zone satisfactorily, model 3 underpredicted the width of the necrotic zone. On the other hand, Figure 7b shows that model 3 predicted the depth of the necrotic zone quite well at the centerline ( $r = 0$ ). As for the simulations shown in Figure 6, Figure 7b shows that the thermally affected region was larger for model 3, but the actual shape of the necrotic zone was different from that predicted with this model. Figure 7a,b reveals that our numerical code is capable of accurately predicting the ablation crater shape and size, but the thermal damage models examined in this study fail to accurately predict the thermally damaged areas, especially the necrotic zone. Clearly, the issues of model selection and model calibration come

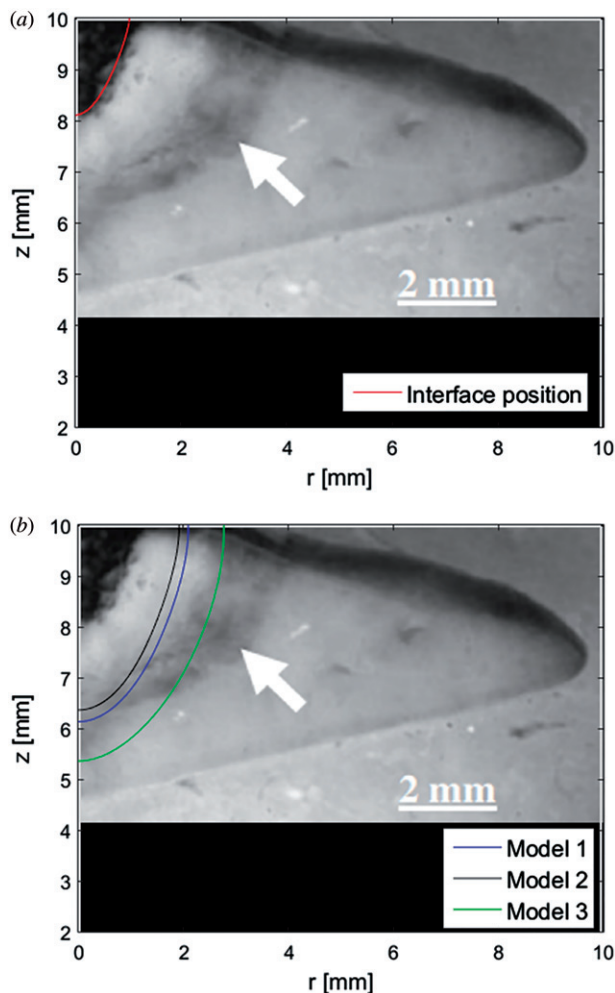


**Figure 7.** (a) Ablation interface position compared with ablation lesion crater [16] and (b) thermal damage region after 10 s of heating compared with white/dark zone [16].

into picture, in order to obtain a more accurate representation of the phenomena involved in the thermal damage of biological tissues during ablation by a laser.

## Conclusions

The bioheat transfer problem during the thermal ablation of biological tissues was numerically solved in this work. The finite volume method was used for the numerical solution together with the VOF method, which was applied to track the moving boundary that results from the material removal by a steady laser beam when the tissue surface reaches high temperatures. The code and the numerical solution were verified in accordance with ASME standards, resulting in a small GCI. A comparison of the numerical results obtained in this work with experimental data available in the literature for the ablation of rat liver reveals an excellent agreement for the crater position and shape. Therefore, the code developed in this work can be used for the accurate prediction of the tissue removal caused by a laser during the ablation of biological tissues. On the other hand, the thermal damage models examined in this study

could not accurately predict the sizes and shapes of experimentally measured coagulation and necrotic zones. Inverse analysis techniques are needed for model selection and model calibration, in order to accurately predict such thermally affected zones during laser ablation treatments.

## Acknowledgments

The support provided by CNPq, CAPES, and FAPERJ, agencies of the Brazilian and Rio de Janeiro state governments, is gratefully appreciated.

## ORCID

Bruna R. Loiola  <http://orcid.org/0000-0002-8314-7002>  
 Helcio R. B. Orlande  <http://orcid.org/0000-0002-3511-322X>  
 George S. Dulikravich  <http://orcid.org/0000-0003-3292-2723>

## References

- [1] A. J. Welch, J. W. Valvano, J. A. Pearce, L. J. Hayes, and M. Motamedi, "Effect of laser radiation on tissue during laser angioplasty," *Lasers Surg. Med.*, vol. 5, pp. 251–264, 1985. DOI: [10.1002/lsm.1900050307](https://doi.org/10.1002/lsm.1900050307).
- [2] F. Partovi *et al.*, "A model for thermal ablation of biological tissue using laser radiation," *Lasers Surg. Med.*, vol. 7, pp. 141–154, 1987. DOI: [10.1002/lsm.1900070202](https://doi.org/10.1002/lsm.1900070202).
- [3] A. Vogel and V. Venugopalan, "Mechanisms of pulsed laser ablation of biological tissues," *Chem. Rev.*, vol. 103, pp. 577–644, 2003. DOI: [10.1021/cr030683b](https://doi.org/10.1021/cr030683b).
- [4] C. Brace, "Thermal tumor ablation in clinical use," *IEEE Pulse*, vol. 2, no. 5, pp. 28–38, 2011. DOI: [10.1109/MPUL.2011.942603](https://doi.org/10.1109/MPUL.2011.942603).
- [5] S. N. Goldberg *et al.*, "Image-guided tumor ablation: standardization of terminology and reporting criteria," *Radiology*, vol. 235, no. 3, pp. 728–739, 2005. DOI: [10.1148/radiol.2353042205](https://doi.org/10.1148/radiol.2353042205).
- [6] K. F. Chu and D. E. Dupuy, "Thermal ablation of tumours: biological mechanisms and advances in therapy," *Nat. Rev. Cancer*, vol. 14, pp. 199–208, 2014. DOI: [10.1038/nrc3672](https://doi.org/10.1038/nrc3672).
- [7] R. W. Habash, R. Bansal, D. Krewski, and H. T. Alhafid, "Thermal therapy, part III: ablation techniques," *Crit. Rev. Biomed. Eng.*, vol. 35, no. (1–2), pp. 37–121, 2007. DOI: [10.1615/CritRevBiomedEng.v35.i1-2.20](https://doi.org/10.1615/CritRevBiomedEng.v35.i1-2.20).
- [8] F. Morady, "Radio-frequency ablation as treatment for cardiac arrhythmias," *N. Engl. J. Med.*, vol. 340, no. 7, pp. 534–544, 1999. DOI: [10.1056/NEJM199902183400707](https://doi.org/10.1056/NEJM199902183400707).
- [9] Y.F. Zhou, "High intensity focused ultrasound in clinical tumor ablation," *W. J. Clin. Oncol.*, vol. 2, no. 1, pp. 8–27, 2011. DOI: [10.5306/wjco.v2.i1.8](https://doi.org/10.5306/wjco.v2.i1.8).
- [10] H. H. Pennes, "Analysis of tissue and arterial blood temperatures in the resting human forearm," *J. Appl. Physiol.*, vol. 1, no. 2, pp. 93–122, 1948. DOI: [10.1152/jappl.1948.1.2.93](https://doi.org/10.1152/jappl.1948.1.2.93).
- [11] J. P. Abraham and E. M. Sparrow, "A thermal-ablation bioheat model including liquid-to-vapor phase change, pressure- and necrosis-dependent perfusion, and moisture-dependent properties," *Int. J. Heat Mass Transf.*, vol. 50, pp. 2537–2544, 2007. DOI: [10.1016/j.ijheatmasstransfer.2006.11.045](https://doi.org/10.1016/j.ijheatmasstransfer.2006.11.045).
- [12] F. C. Henriques Jr. and A. R. Moritz, "Studies of thermal injury. I. The conduction of heat to and through skin and the temperatures attained therein: a theoretical and an experimental investigation," *Am. J. Pathol.*, vol. 23, pp. 531–549, 1947.
- [13] A. R. Moritz and F. C. Henriques Jr., "Studies of thermal injury: II. The relative importance of time and surface temperature in the causation of cutaneous burns," *Am. J. Pathol.*, vol. 23, no. 5, pp. 695–720, 1947.
- [14] A. R. Moritz, "Studies of thermal injury: III. The pathology and pathogenesis of cutaneous burns: an experimental study," *Am. J. Pathol.*, vol. 23, no. 6, pp. 915–941, 1947.
- [15] F. C. Henriques Jr., "Studies of thermal injury: V. The predictability and the significance of thermally induced rate processes leading to irreversible epidermal injury," *Arch. Pathol.*, vol. 43, no. 5, pp. 489–502, 1947.
- [16] S. L. Thomsen and J. A. Pearce, "Thermal damage and rate processes in biological tissues," in *Optical-Thermal Response of Laser-Irradiated Tissue*, 2nd ed., chap. 13, A. J. Welch and M. J. C. VanGemert, Eds. Dordrecht, Netherlands: Springer Science + Business Media B.V., 2011, pp. 487–549.
- [17] N.T. Wright, "Quantitative models of thermal damage to cells and tissues," in *Heat Transfer and Fluid Flow in Biological Processes*, chap. 3, S. M. Becker and A. V. Kuznetsov, Eds. Amsterdam, NY, USA: Elsevier, 2015, pp. 59–76.



- [18] J. A. Pearce, S. L. Thomsen, H. Vijverberg, and T. J. McMurray, "Kinetics for birefringence changes in thermally coagulated rat skin collagen," *Proc. SPIE.*, vol. 1876, pp. 180–186, 1993. DOI: [10.1117/12.147029](https://doi.org/10.1117/12.147029).
- [19] J. A. Pearce, "Comparative analysis of mathematical models of cell death and thermal damage process," *Int. J. Hyperthermia*, vol. 29, no. 4, pp. 262–280, 2013. DOI: [10.3109/02656736.2013.786140](https://doi.org/10.3109/02656736.2013.786140).
- [20] C. E. Weir, "Rate of shrinkage of tendon collagen: heat, entropy, and free energy of activation of the shrinkage of untreated tendon; effect of acid, salt, pickle, and tannage on the activation of tendon collagen," *J. Res. Natl. Bur. Stand.*, vol. 42, pp. 17–32, 1949. DOI: [10.6028/jres.042.002](https://doi.org/10.6028/jres.042.002).
- [21] S. S. Chen, N. T. Wright, and J. D. Humphrey, "Phenomenological evolution equations for heat-induced shrinkage of a collagenous tissue," *IEEE Trans. Biomed. Eng.*, vol. 45, no. 10, pp. 1234–1240, 1998. DOI: [10.1109/10.720201](https://doi.org/10.1109/10.720201).
- [22] S. S. Chen, N. T. Wright, and J. D. Humphrey, "Heat-induced changes in the mechanics of a collagenous tissue: isothermal free shrinkage," *ASME J. Biomech. Eng.*, vol. 119, no. 4, pp. 372–378, 1997. DOI: [10.1115/1.2798281](https://doi.org/10.1115/1.2798281).
- [23] M. S. Wall, X-H Deng, P. A. Torzilli, S. B. Doty, S. J. O'Brien, and R. F. Warren, "Thermal modification of collagen," *J. Shoulder Elbow Surg.*, vol. 8, no. 4, pp. 339–344, 1999. DOI: [10.1016/S1058-2746\(99\)90157-X](https://doi.org/10.1016/S1058-2746(99)90157-X).
- [24] J. A. Pearce, I. Çilesiz, A. J. Welch, E. Chan, T. McMurray, and S. Thomsen, "Comparison of Ho:YAG, Tm:YAG and argon lasers for fusion of intestinal tissues," *Proc. SPIE.*, vol. 2128, pp. 517–526, 1994. DOI: [10.1117/12.184938](https://doi.org/10.1117/12.184938).
- [25] H. A. Johnson and M. Pavelec, "Thermal injury due to normal body temperature," *Am. J. Pathol.*, vol. 66, pp. 557–564, 1972.
- [26] W. C. Dewey, L. E. Hopwood, S.A. Sapareto, and L. E. Gerweck, "Cellular responses to combinations of hyperthermia and radiation," *Radiology*, vol. 123, pp. 463–479, 1977. DOI: [10.1148/123.2.463](https://doi.org/10.1148/123.2.463).
- [27] G.M. Hahn, *Hyperthermia and Cancer*. New York, NY: Plenum Press, 1982.
- [28] J. L. Roti Roti and K. J. Henle, "Comparison of two mathematical models for describing heat-induced cell killing," *Radi. Res.*, vol. 81, pp. 374–83, 1980. DOI: [10.2307/3575196](https://doi.org/10.2307/3575196).
- [29] Y. Feng, J. T. Oden, and M. N. Rylander, "A two-state cell damage model under hyperthermic conditions: theory and *in vitro* experiments," *J. Biomech. Eng.*, vol. 130, no. 4, pp. 1–13, 2008. DOI: [10.1115/1.2947320](https://doi.org/10.1115/1.2947320).
- [30] D.P. O'Neill *et al.*, "A three-state mathematical model of hyperthermic cell death," *Ann. Biomed. Eng.*, vol. 39, pp. 570–579, 2011. DOI: [10.1007/s10439-010-0177-1](https://doi.org/10.1007/s10439-010-0177-1).
- [31] S. L. Thomsen, "Mapping of thermal injury in biologic tissues using quantitative pathologic techniques," *Proc. SPIE.*, vol. 3594, pp. 82–95, 1999. DOI: [10.1117/12.348748](https://doi.org/10.1117/12.348748).
- [32] S. L. Thomsen and J. A. Pearce, "Temperatures associated with thermally induced red blood cell changes in tissues irradiated *in vivo*," *Proc. SPIE.*, vol. 2130, pp. 156–163, 1994 DOI: [10.1117/12.179925](https://doi.org/10.1117/12.179925).
- [33] A. J. Welch *et al.*, "Laser probe ablation of normal and atherosclerotic human aorta *in vitro*: a first thermographic and histologic analysis," *Circulation.*, vol. 76, no. 6, pp. 1353–1363, 1987. DOI: [10.1161/01.CIR.76.6.1353](https://doi.org/10.1161/01.CIR.76.6.1353).
- [34] S. V. Patankar, *Numerical Heat Transfer and Fluid Flow*, New York, NY: Hemisphere Publishing Corporation, 1980.
- [35] M. N. Ozisik, H. R.B. Orlande, M. J. Colaço, and R. M. Cotta, *Finite Difference Methods in Heat Transfer*, vol. 2, 2nd ed. Boca Raton, FL: CRC Press, 2017, p.564.
- [36] C. W. Hirt and B. D. Nichols, "Volume of fluid (VOF) method for the dynamics of free boundaries," *J. Comput. Phys.*, vol. 39, pp. 201–225, 1981. DOI: [10.1016/0021-9991\(81\)90145-5](https://doi.org/10.1016/0021-9991(81)90145-5).
- [37] S. W. J. Welch and J. Wilson, "A volume of fluid based method for fluids flows with phase change," *J. Comput. Phys.*, vol. 160, pp. 662–682, 2000. DOI: [10.1006/jcph.2000.6481](https://doi.org/10.1006/jcph.2000.6481).
- [38] N. J. Ruperti Jr. and R. M. Cotta, *Heat Conduction with Ablation in Multilayered Media*, 11th Brazilian Congress of Mechanical Engineering. São Paulo: XI COBEM, 1991, pp. 413–416.
- [39] I. B. Celik, U. Ghia, and P. J. Roache, "Procedure for estimation and reporting of uncertainty due to discretization in CFD applications," *J. Fluids Eng.*, vol. 130, pp. 1–4, 2008. DOI: [10.1115/1.2960953](https://doi.org/10.1115/1.2960953).
- [40] Standard for Verification and Validation in Computational Fluid Dynamics and Heat Transfer, Chap. 2, ASME V&V 20, 2009.
- [41] J. H. Lambert, *Photometry or On the Measure and Gradations of Light, Color, and Shade*, Translate by David L. DiLaura, Augsburg, Illuminating Engineering Society, 2001.
- [42] S. L. Jacques and S. A. Prahl, "Modelling optical and thermal distributions in tissue during laser irradiation," *Lasers Surg. Med.*, vol. 6, no. 6, pp. 494–503, 1987. DOI: [10.1002/lsm.1900060604](https://doi.org/10.1002/lsm.1900060604).
- [43] D. L. Youngs, "Time-dependent multi-material flow with large fluid distortion," in *Numerical Methods for Fluids Dynamics*, K. W. Morton and M. J. Baines, Eds. New York, NY: Academic Press, 1982, pp. 273–285.
- [44] D. L. Youngs, "An interface tracking method for a 3D Eulerian hydrodynamics code," *Atomic Weapon Research Establishment*, 1984.
- [45] H. H. Mitchell, T. S. Hamilton, F. R. Steggerda, and H. W. Bean, "The chemical composition of the adult human body and its bearing on the biochemistry of growth," *J. Biol. Chem.*, vol. 158, pp. 625–637, 1945.

- [46] T. E. Cooper and G. J. Trezek, Correlation of thermal properties of some human tissues with water content. *Aerospace Med.*, vol. 42, no. 1, pp. 24–27, 1971.
- [47] J. A. Pearce, “Numerical models of laser fusion of intestinal tissues,” presented at the 31st Annu. Inter. Confer. of the IEEE EMBS. Minnesota, USA, pp. 4303–4306, Sep 2009. DOI: [10.1109/IEMBS.2009.5333797](https://doi.org/10.1109/IEMBS.2009.5333797).
- [48] P. Parsa, S. L. Jacques, and N. S. Nishioka, “Optical properties of rat liver between 350 and 2200 nm,” *Applied Optics*, vol. 28, no. 12, pp. 2325–2330, 1989. DOI: [10.1364/AO.28.002325](https://doi.org/10.1364/AO.28.002325).
- [49] K. Matthewson, P. Coleridge-Smith, J. P. O’Sullivan, T. C. Northfield, and S. G. Bown, “Biological effects of intrahepatic neodymium: yttrium-aluminum-garnet laser photocoagulation in rats,” *Gastroenterology.*, vol. 93, pp. 550–557, 1987. DOI: [10.1016/0016-5085\(87\)90918-8](https://doi.org/10.1016/0016-5085(87)90918-8).
- [50] M. J. Moran and H. N. Shapiro, *Fundamentals of Engineering Thermodynamics*, 5th ed. New York, NY: John Wiley & Sons, Inc., 2006, p.721.
- [51] T. L. Bergman, A. S. Lavine, F. P. Incropera, and D. P. DeWitt, *Fundamentals of Heat and Mass Transfer*, 7th ed. New York, NY: John Wiley & Sons, Inc., 2011.